ELSEVIER

Contents lists available at ScienceDirect

Electrochimica Acta

journal homepage: www.journals.elsevier.com/electrochimica-acta





Continuum insight into the effects of electrode design parameters on the electrochemical performance of lithium-ion batteries

Williams Agyei Appiah ^{a, c, *}, Dohwan Kim ^b, Yong Min Lee ^b, Juan Maria Garcia-Lastra ^a, Ivano E. Castelli ^{a, *}

- a Department of Energy Conversion and Storage, Technical University of Denmark, DK-2800 Kgs. Lyngby, Denmark
- b Department of Energy Science and Engineering, Daegu Gyeongbuk Institute of Science and Technology (DGIST), 333 Techno Jungang-daero, Dalseong-gun, Daegu 42988. Republic of Korea
- ^c Department of Engineering Sciences, University of Agder, 4879 Grimstad, Norway

ARTICLE INFO

Keywords: Li-ion batteries Continuum scale models Electrode design optimization Pseudo-two-dimensional model

ABSTRACT

Lithium-ion batteries energy and power density strongly depend on the type of active material and the electrode design parameters. An in-depth understanding of the effect of battery design parameters on their electrochemical performance is experimentally expensive and hence requires the utilization of cheaper continuum scale models. Here, using a lithium-ion cell composed of LiFePO₄ cathode, $\rm Li_4Ti_5O_{12}$ anode and a porous separator filled with a liquid electrolyte as an example, we demonstrate the use of an experimentally validated pseudo-two-dimensional (P2D) model in one-dimension to explore the effects of different cell design parameters on the discharge capacity at different current rates. The model is simulated in two-dimensional to instantly visualize the concentration distribution of Li ions in the electrode at high discharge current rates. The continuum model unravels that the solution phase diffusion limitation is the main factor inhibiting the performance of thick electrodes at high current rates and the $\rm Li_4Ti_5O_{12}$ anode is the limiting electrode. These findings using continuum models provide guidance for and accelerate the optimization of electrode architecture for enhancing the performance of lithium-ion batteries.

1. Introduction

Lithium-ion batteries (LIBs) are the most dominant battery technology used in portable electronic devices, electric vehicles, and residential systems due to their high specific energy density, long cycle life, low and decreasing costs [1-3]. However, the ever-growing demand of energy storage for electric vehicles requires that the energy density of current commercial LIBs should be increased from 200 –250 Wh kg⁻¹ to about 350 Wh kg⁻¹ at the cell level (short term goals). Considering that these requirements are just the short-term goals, meeting the long-term goal of 500 Wh kg⁻¹ with over 1000 cycles [4] would demand the discovery of high energy density cathode materials. An alternative practical approach involves increasing the loading amount of the active materials and the thickness of the electrodes, which leads to a decrease in the volume fraction of the inactive components (packaging, separator, and current collectors). Increasing the thickness of the cathode enhances the specific energy of LIBs to a greater extent [5-7], however cathode thickness above 50 µm results in sluggish electronic and ionic transportation networks [8,9] which affects the operation heterogeneity and electrode performance under high voltage cycling conditions [10, 11]

To categorically study and predict the effect of various electrode designs, in particular the thickness of the cathode, anode, and separator on the rate performance of LIBs in a cheap and time effective way, a high fidelity experimentally validated continuum model is desirable [12–14]. This is because over the years continuum models have proven to be effective in explaining the electrochemical characteristics and predicting cycle performance of batteries with different electrode configuration and composition [15–20]. For instance, 1D continuum physics-based models have been used to unravel the effect of cathode thickness and porosities on the transport of Li ions [5,6] and explain the plating-stripping mechanisms in batteries [21–24]. Moreover, continuum models have been adopted to design and optimize natural graphite/LiFePO₄ full cells [25] and Li/LiNiO_{1/3}Mn_{1/3}Co_{1/3}O₂ half cells [26] by varying the thickness and porosity of the cathode. Recently, Li et al. revealed the impact of the thickness and porosity of separator on the

E-mail addresses: williams.a.appiah@uia.no (W.A. Appiah), ivca@dtu.dk (I.E. Castelli).

^{*} Corresponding authors.

Table 1Cell design parameters used for the simulation.

Parameters	Symbol	LiFePO ₄	LiTi ₅ O ₁₂
Electrode thickness, μm ^a	L_i	30, 40, 50	68
Volume fraction electrolyte ^a	$arepsilon_{\mathit{S},i}$	0.2	0.3
Reaction rate constant, mol/m ² s ^c	k_i^0	8×10^{-10}	8×10^{-10}
Maximum concentration, mol m ^{-3a}	$c_{s,i}^{max}$	22,836	22,852
Electrode conductivity, S/m ^b	σ_{1i}	10	100
Separator thickness, μm ^a	L_{sep}	20, 40, 60	
Separator porosity ^a	$arepsilon_{\mathit{Sep}}$	0.37	
Initial salt concentration, M ^a	c_l^0	1.15	
Diffusion coefficient, m ² /s ^b	$D_{1,i}^0$	3.0×10^{-14}	1.15×10^{-14}
Particle radius, µm ^a	r_i	1.7	0.5
Diffusion coefficient in electrolyte, m ² /s ^d	$D_{2.i}^0$	3.0×10^{-10}	
Ionic conductivity of electrolyte, S/m d	σ_{2i}	0.927	
Transference number ^d	t^+	0.363	

^a Parameters set in cell design.

 Table 2

 Comparison data for cells with different cathode and separator thickness.

	Separator thickness (μm)			
Parameter	20	40	60	
30 μm cathode thickness				
x^{0a}	0.990	0.990	0.990	
y^{0a}	0.001	0.001	0.001	
1C rate (mA cm ⁻²)	1.030	1.030	1.030	
R contact (Ω cm ²) ^a	0.975	0.975	0.975	
40 μ m cathode thickness				
$\mathbf{x^{0a}}$	0.990	0.990	0.990	
y ^{0a}	0.001	0.001	0.001	
1C rate (mA cm ⁻²)	1.370	1.370	1.370	
$R_{contact} (\Omega cm^2)^a$	0.625	0.625	0.625	
50 μ m cathode thickness				
$\mathbf{x^{0a}}$	0.990	0.990	0.980	
y^{0a}	0.001	0.001	0.001	
1C rate (mA cm ⁻²)	1.720	1.720	1.720	
$R_{contact} (\Omega cm^2)^a$	0.440	0.440	0.440	

^a Fitted.

electrochemical performance of 38,120-type graphite/LiFePO₄ battery using an electrochemical-thermal coupled model [27]. Previous reports in literature usually consider the optimization of LIBs with respect to either the cathode or the separator or the anode, but not all three simultaneously. In addition, all the above listed works considered graphite anode-based LIBs, thus there are limited reports on modeling-based optimization of LIBs employing $\text{Li}_4\text{Ti}_5\text{O}_{12}$ as the anode. Moreover, the visualization of Li ions concentration distribution in the cathode at high current rates is not well demonstrated.

The objective of this study is to analyze how variations in electrode and separator thicknesses and porosities impact the electrochemical performance of LIBs using a validated continuum physics-based model. Battery cells comprising varying thicknesses and porosities of LiFePO4 cathode, Celgard separator, and $\rm Li_4Ti_5O_{12}$ anode were employed to generate voltage profiles at different current rates to validate a one-dimensional (1D) continuum model. The model is extended to a two-dimensional model (2D) to simulate the concentration distribution of Li ions in the three domains (cathode, separator, and anode) of the cell at a high current rate. To gain insights on the simultaneous effect of different cell designs on the rate performance, we used the validated model to predict the discharge capacities at different current rates and electrode thickness as a function of the separator thickness. This study reveals the limitations of thick electrodes and separators especially at high current rates. The data generated and the model used in this study

is converted into a COMSOL Multiphysics-based app and made readily available for designing and optimizing different electrode designs [28].

2. Model development

The data presented in this work was obtained from continuum model simulation of a lithium-ion cell consisting of an ${\rm Li_4Ti_5O_{12}}$ anode and an LiFePO₄ cathode. The porous part of the electrodes was assumed to be filled by a liquid electrolyte whose transport and kinetic properties as well as the parameters used for the simulation are given in Tables 1 and 2. The initial concentration of the electrolyte was assumed to be uniform across the cell. The pseudo two-dimensional (P2D) model developed by Newman et al. [29,30] and used widely many researchers [5,15,31–36] was adopted to model the electrochemical performance of the cell in 1D and 2D. The main purpose for performing this simulation in 2D was to understand the variation of different electrode thickness visually and instantly on the various concentration profiles across the cells. The model equations used in this study are similar to those described previously by [37] and hence are not listed in this paper.

In general, the P2D model relies on accounting for material balances within the solid phase of both electrodes and the liquid electrolyte. This encompasses the participation of Li ions in all reactions as well as adherence to Ohm's law in both the solid and liquid phases. The electrochemical processes transpiring at the electrode surfaces were elucidated through the Butler-Volmer equation, specifically designed for Liion intercalation and deintercalation reactions. The collection of equations employed in the P2D model, along with their associated boundary conditions, can be found in Table 3. Notably, the model omits energy balance equations due to the simulations being conducted at low current densities. At such levels, the temperature distribution across the cell remains relatively constant under a given operational temperature. The simulation was executed using the COMSOL Multiphysics lithium-ion battery module. The simulation set up of the cell modeled in this study is presented in Fig. 1.

3. Experiments

Electrode Preparation and Cell Assembly: The cathode composition was set to 90 wt% LiFePO₄ (LFP, Hanhwa Solutions, Korea), 5 wt% polyvinylidene fluoride binder (PVdF, KF-1300, Mw = 350,000, Kureha Co., Japan), and 5 wt% conductive carbon (Super P ® Li, Imerys, Belgium). An *N*-methyl-2-pyrrolidone (NMP, Sigma-Aldrich, U.S.A.) slurry having all the electrode components was cast on an Al current collector foil (15 μm, Sam-A Aluminum, Korea). The coated slurry on the Al foil was first dried in an oven at 130 °C for 1 h and then roll-pressed to a targeted

^b Parameters based on literature value [37].

^c Fitted parameter.

^d Obtained from COMSOL library.

Table 3 Pseudo-two-dimensional model governing equations for LiFePO $_4$ / Li $_4$ Ti $_5$ O $_{12}$ cell.

Region		Governing equations	Eq. No.	Boundary or initial condition
Anode	Diffusion in solid particles	$\frac{\partial c_{1,n}}{\partial t} = D_{1,n} \frac{1}{r^2} \frac{\partial}{\partial r} \left(r^2 \frac{\partial c_{1,n}}{\partial r} \right)$	E1	$c_{1,n}(r,0) _{t=0} = c_{1,n}^0 - D_{1,n} \frac{\partial c_{1,n}}{\partial r} _{r=0} = 0, -D_{1,n} \frac{\partial c_{1,n}}{\partial r} _{r=R_{p,n}} = j_n$
	Potential in solid phase	$\sigma_{1,n}^{eff} rac{\partial^2 \Phi_{1,n}}{\partial v^2} = a_{1,n} F j_n$	E2	$\left.\sigma_{1,n}\right _{x=L_n} = 0 - \sigma_{1,n} \frac{\partial \Phi_{1,n}}{\partial x} _{x=0} = 0$
	Material balance in solution phase	$\varepsilon_{2n}\frac{\partial c_{2n}}{\partial t} = \frac{\partial}{\partial x} \left(\varepsilon_1^{1.5} D_{2,n} \frac{\partial c_{2n}}{\partial x} \right) + \left(1 - t_+^0 \right) a_{1,n} j_n$	E3	$c_1 _{t=0} = c_1^0 - D_{2,n} \frac{\partial c_{2,n}}{\partial x} _{x=0} = \frac{I_{app}(1-t_+)}{F}, D_{2,n} \frac{\partial c_{2,n}}{\partial x} _{x=L_n} =$
	Potential in solution phase	$-\frac{\partial}{\partial x}\left(\varepsilon_{2,n}^{1.5}\kappa\frac{\partial\phi_{2,n}}{\partial x}\right) + \frac{2RT(1-t_{+}^{0})}{F}\frac{\partial}{\partial x}\left(\varepsilon_{2,n}^{1.5}\kappa\frac{\partial\ln c_{2}}{\partial x}\right) =$	E4	$D_{2,sep} rac{\partial \mathcal{C}_{2,n}}{\partial x} _{x=L_n}$ $\kappa_n rac{\partial \Phi_{2,n}}{\partial x} _{x=L_n} = 0, \kappa_n rac{\partial \Phi_{2,n}}{\partial x} _{x=L_n} = \kappa_{sep} rac{\partial \Phi_{2,sep}}{\partial x} _{x=L_n}$
	Butler-Volmer kinetics	$j_n = \frac{i_n^0}{F} \left[\exp\left(\frac{0.5F}{RT}\eta_n^{at}\right) - \exp\left(-\frac{0.5F}{RT}\eta_n^{at}\right) \right]$	E5	-
		$i_n^0 = Fk_n (c_{1,n,\max} - c_{1,n,surf})^{0.5} c_{1,n,surf}^{0.5} c_{2,n}^{0.5}$	E6	-
		$\eta_n^{ct} = \Phi_{1,n} - \Phi_{2,n} - U_n^0$	E7	-
	OCV	$U_n^0 = 0.8470 \exp(-78.7354SOC)$ +1.5595 \exp(-0.0152SOC)	E8	
Separator	Material balance in solution phase	$ \varepsilon_{sep} \frac{\partial c_2}{\partial t} = \frac{\partial}{\partial x} \left(\varepsilon_{sep}^{1.5} D_{2,sep} \frac{\partial c_2}{\partial x} \right) $	E9	$c_2 _{t=0} = c_2^0 \; D_{2,n} \frac{\partial c_2}{\partial x} _{x=L_n} = D_{2,sep} \frac{\partial c_2}{\partial x} _{x=L_n} \; D_{2,sep} \frac{\partial c_2}{\partial x} _{x=L_s} \; = \;$
				$D_{2p} \frac{\partial c_2}{\partial x} _{x=L_s}$
	Potential in solution phase	$-e_{sep}^{1.5}\kappa \frac{\partial \phi_{2,sep}}{\partial x} + \frac{2RT(1-t_+^0)}{E}e_{sep}^{1.5}\kappa \frac{\partial \ln c_2}{\partial x} = 0$	E10	$\kappa_{sep} \frac{\partial \Phi_{2,sep}}{\partial x} _{x=L_p} = \kappa_p \frac{\partial \Phi_{2,p}}{\partial x} _{x=L_p} - \kappa \frac{\partial \Phi_{2,n}}{\partial x} _{x=L_n} = -\kappa \frac{\partial \Phi_{2,sep}}{\partial x} _{x=L_s}$
Cathode Diffusion in solid partic	Diffusion in solid particles	$\frac{\partial c_{1,p}}{\partial t} = D_{1,p} \frac{1}{r^2} \frac{\partial}{\partial r} \left(r^2 \frac{\partial c_{1,p}}{\partial r} \right)$	E11	$c_{1p}(r,0) _{t=0} = c_{1p}^0 - D_{1p} \frac{\partial c_{1p}}{\partial r} _{r=0} = 0 - D_{1p} \frac{\partial c_{1p}}{\partial r} _{r=R_{pp}} = j_p$
	Potential in solid phase	$\epsilon_{1p}^{1.5}\sigma_{1p}\frac{\partial^2\Phi_{1p}}{\partial v^2}=a_{1p}Fj_p$	E12	$-\sigma_{1,p}rac{\partial\Phi_{1,p}}{\partial x} _{x=L_{s}}=0-\sigma_{1,p}rac{\partial\Phi_{1,p}}{\partial x} _{x=L_{p}}=I_{app}$
Material balance in solution phase Potential in solution phase Butler-Volmer kinetics Diffusion coefficient Reaction rate constant OCV	$arepsilon_{2p}rac{\partial c_{2,p}}{\partial t} = rac{\partial}{\partial x} \left(arepsilon_1^{1.5} D_2 rac{\partial c_{2,p}}{\partial x} ight) + \left(1 - t_+^0 ight) a_{1,p} j_p$	E13	$-D_{2,p}rac{\partial c_{2,p}}{\partial x} _{x=L_p}=0, D_{2,sep}rac{\partial c_{2,p}}{\partial x} _{x=L_s}=D_{2,p}rac{\partial c_{2,p}}{\partial x} _{x=L_s}$	
	•	$-\frac{\partial}{\partial x}\left(\kappa_{eff,p}\frac{\partial \Phi_{2,p}}{\partial x}\right) + \frac{2RT(1-t_+^0)}{F}\frac{\partial}{\partial x}\left(\kappa_{eff,p}\frac{\partial \ln c}{\partial x}\right) = a_1j_pF_0$	E14	$-\kappa_p \frac{\partial \Phi_{2,p}}{\partial x} _{x=L_p} = 0\kappa_p \frac{\partial \Phi_{2,p}}{\partial x} _{x=L_p} = \kappa_{\text{sep}} \frac{\partial \Phi_{2,\text{sep}}}{\partial x} _{x=L_z}$
	$j_p = \frac{i_p^0}{F} \left[\exp\left(\frac{0.5F}{RT}\eta_p\right) - \exp\left(-\frac{0.5F}{RT}\eta_p\right) \right]$	E15	-	
		$i_p^0 = Fk_p (c_{1,p,\max} - c_{1,p,sterf})^{0.5} c_{1,p,sterf}^{0.5} c_{2,p}^{0.5}$	E16	-
		$ \eta_{p}^{ct} = \Phi_{1,p} - \Phi_{2,p} - U_{0}^{0} $	E17	_
	$D_{1,p} = \frac{D_{1,p}^0}{(1 + SOC)^{1.6}}$	E18		
	Reaction rate constant	$k_p = k_p^0 \exp(-3 \times SOC)$	E19	
		$U_p^0 = 3.5 + 0.65811 \tanh(2.8080SOC + 0.1278)$	E20	
		$-\left(1/(1-SOC)^{0.14}\right) - 0.0130\exp(5.2620SOC^8)$		
		$+0.4405\exp(-4(SOC - 0.0834))$		
Battery	Output voltage	$V_{\mathrm{batt}} = \Phi_1 _{x=L_p} - \Phi_1 _{x=0} - R_f I_{app}$	E21	-

thickness using a gap-control-type pressing machine (CIS, Korea). The anode was prepared by the same procedure as the cathode with composition of 90 wt% Li₄Ti₅O₁₂ (LTO, Posco Chemical, Korea), 5 wt% PVdF, 5 wt% conductive carbon, and Cu collector foil (10 μm , Iljin Materials, Korea). LiFePO₄/Li₄Ti₅O₁₂ cell was assembled in the glovebox using 2032-type coin cell parts. As the liquid electrolyte, a mixture of 1.15 M LiPF₆ in ethylene carbonate/ethyl methyl carbonate (EC/EMC = 3/7, v/v, ENCHEM, Korea) was used without further purification. Depending on the experimental conditions, 1, 2 or 3 sheets of polyethylene separator (20 μm , F20BHE, Toray, Japan) was used. All the coin cells were aged over 12 h before electrochemical characterization.

Electrochemical measurements: The rate capability of LiFePO $_4$ / Li $_4$ Ti $_5$ O $_{12}$ cells was evaluated by increasing the discharging c-rate from 0.5 to 10C (constant current, CC mode, 0.5, 1, 2, 3, 5, 10 and 0.5C), while maintaining the charging current c-rate at 0.5C (constant current/constant voltage, CC/CV mode, cutoff current: 0.1C) between 1.0 and 2.5 V. Each cycle was repeated five times in a temperature-controlled chamber at 25 °C using a TOSCAT-3100 series battery test system (TOYO SYSTEM Co., LTD., Japan).

4. Results and discussion

4.1. Experiments

To understand the effect of the distance between the cathode and the anode, and the thickness of the cathode on the electrochemical performance of LIBs, we studied the rate capabilities of LiFePO₄/Li₄Ti₅O₁₂ cells with separator and cathode of various thicknesses and presented the outcome in Fig. 2. Regardless of the thicknesses of the separator and cathode, all the cells showed similar capacity retention at lower c-rates of 0.5 C and 1C. Above 1 C, the effect of the distance between the cathode and the anode on the capacity retention became pronounced especially at high C-rates of 5 C and 10 C. As observed in Fig. 2a, b and c, the thickness of the cathode did not have a significant effect on the capacity retention up to 5 C. Nevertheless, the capacity retention was relatively better for the cell with the cathode thickness of 40 μm and a separator thickness of 60 µm (Fig. 2b) than those with cathode thickness of 30 µm (Fig. 2a) and 50 µm (Fig. 2c), and a separator thickness of 60 μm. In principle, cells with thin electrodes exhibit better rate performance than those with thicker electrodes. However, this was not the case for the cells examined in this study and the abnormalities in the

W.A. Appiah et al. Electrochimica Acta 494 (2024) 144470

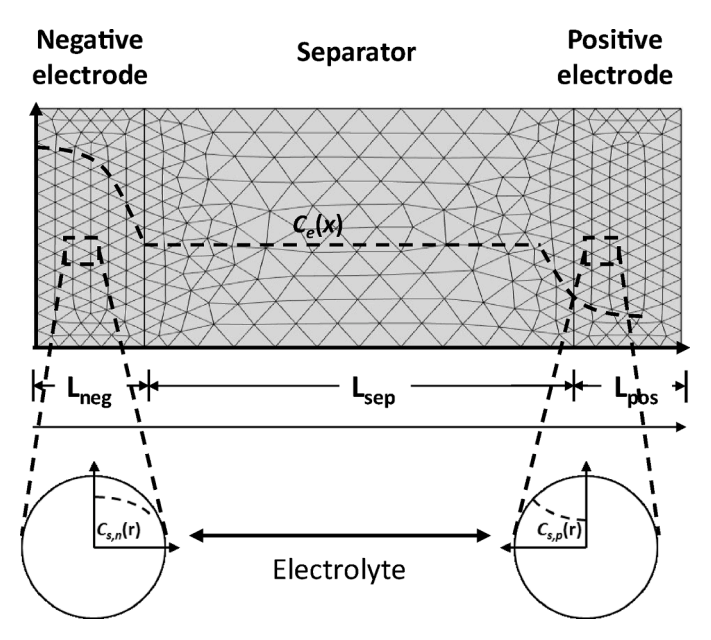


Fig. 1. Schematic diagram of the two-dimensional battery model set up comprising of an ${\rm Li_4Ti_5O_{12}}$ anode and an ${\rm LiFePO_4}$ cathode and 1 M LiPF₆ in EC/EMC (3:7) v/v liquid electrolyte.

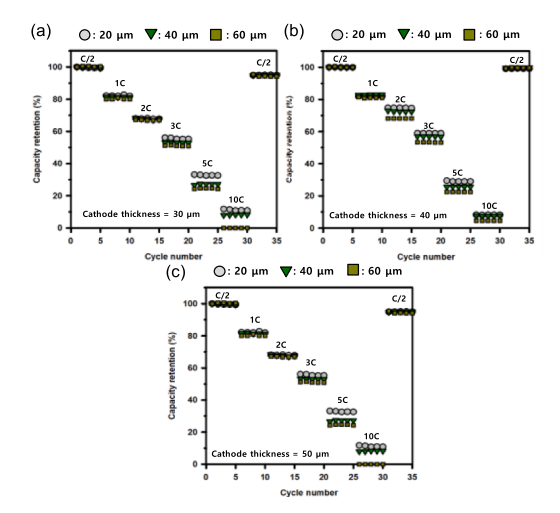


Fig. 2. Rate performance of LiFePO₄/Li₄Ti₅O₁₂ cells with separator thicknesses of 20 μ m, 40 μ m, and 60 μ m, and a cathode thickness of (a) 30 μ m, (b) 40 μ m and (c) 50 μ m.

capacity retention of the thin electrode cells can be attributed to the poor contacts between the active materials and the conductors [38].

4.2. Model validation

To confirm the fidelity of the model, we compared the model predicted discharge voltage profiles to those of experiments obtained from a coin cell consisting of LiFePO₄ cathode and LiTi₅O₁₂ anode at a variety discharge current rate of 0.5 C, 1 C, 2 C, 3 C, 5 C and 10 C and presented the results in Fig. 3. The short dashes represent the simulated results and are based on the cell design parameters in Tables 1 and 2, while the solid lines represent the experimental data at the various discharge current densities. There is a high correlation between the model prediction and the experimental data as observed in Fig. 3. This was achieved by treating the contact resistance (R_{cont}), the initial concentration of Li ions at the surface of the cathode and anode ($c_{s,i}^0$) as fitting parameters. In addition, we expressed the rate constants and diffusion coefficient in the

cathode as a function of the state of charge (SOC) to reflect the two-phase transition behavior of LiFePO $_4$ cathode material. The conditions for the simulation were similar for all the cell designs and the difference was only in the cathode and separator thicknesses. The discharge capacities strongly depended on the discharge current rates. In addition, as the discharge current rates increased, the IR drop in the discharge profiles also increased and the drop was critical at high discharge current rates due to the internal ohmic resistance in the cell. The effect was more pronounced in the cells with longer distance between the cathode and the anode (thicker separators) especially at higher discharge current rate above 2C. However, the cells with a cathode thickness of 40 μm exhibited a smaller IR drop compared to those with cathode thicknesses of 30 μm and 50 μm respectively, making them the optimal cell design.

4.3. Effects of cell design parameters on electrolyte salt concentration

The poor performance of the cells with thicker separators at high discharge rate can be attributed to the large Li ion concentration gradient in the electrodes due to longer diffusion length. To show this effect, we simulated the salt concentration, $c_{2,i}$ (see Eqs. (3), (9) and (13)) at a discharge current rate of 10 C for a variety of cell designs with different cathode and separator thickness. The outcome is presented in Fig. 4. The range of the electrolyte salt concentration as a function of the cell thickness was divided into three parts, namely, high, medium, and low concentration regions. This was achieved by dividing the concentration gradient from the 1D simulation at the end of discharge at 10 C into three parts and using them as an accumulated limit boundary condition for the simulations in 2D. The depth of these concentration regions varied with changes in the thickness of both the separator and cathode. For all the cells, the high electrolyte salt concentration region was within the anode as at the end of discharge. However, the lower boundary of the medium (LBM) or higher boundary of the low (HBL) electrolyte salt concentration region shifted to the front of the separator/ cathode interface as the separator thickness was increased in the cells with a cathode thickness of 30 µm (Fig. 4a and b). The shifting of LBM or HBL became more pronounced as the thickness of the cathode increased in the cells with a separator thickness of 60 µm (Fig. 4d and f). The changes in the shifting of LBM or HBM was not significant as the thickness of the cathode increased in the cells with a separator thickness of 20 µm (Fig. 4c and e). In addition, as observed in the inserted simulated 1D electrolyte salt concentration in Fig. 4, the salt concentration gradient at the end of the 10 C discharge increased with an increase in the thickness of the cathode for a given thickness in the separator. The electrolyte salt concentration reached the critical concentration of 0 mol m^{-3} in the cells with a cathode thickness of 50 μ m (Fig. 4e and f), indicating that, as the cathode thickness increases, solution-phase diffusion limitations become more pronounced at high current densities. This observation is similar to those reported in previous works [5,

4.4. Effects of cell design parameters on Li insertion particle concentration

To understand the impact of solid-phase diffusion limitation on the electrochemical performance of the cell with different electrode designs especially at high discharge current rate, we simulated the Li insertion particle concentration, $c_{1,i}$ (see Eqs. (1) and (11)) at the end of discharge at 10 C and presented the results in Fig. 5. In addition, we calculated the concentrated region which is defined as the region where the Li concentration is above the average concentration in the cathode. This was done to give a visual observation of the depth of Li intercalation in the cathode as a function of the various cell designs. The average concentration was obtained from the simulation in 1D and used as a limit boundary condition in Eqs. (1) and (11) for the simulation in 2D. The simulation in 2D was performed with the limit concentration boundary condition to identify the concentrated region and without the limit concentration boundary. For the cells with similar cathode thickness

Electrochimica Acta 494 (2024) 144470

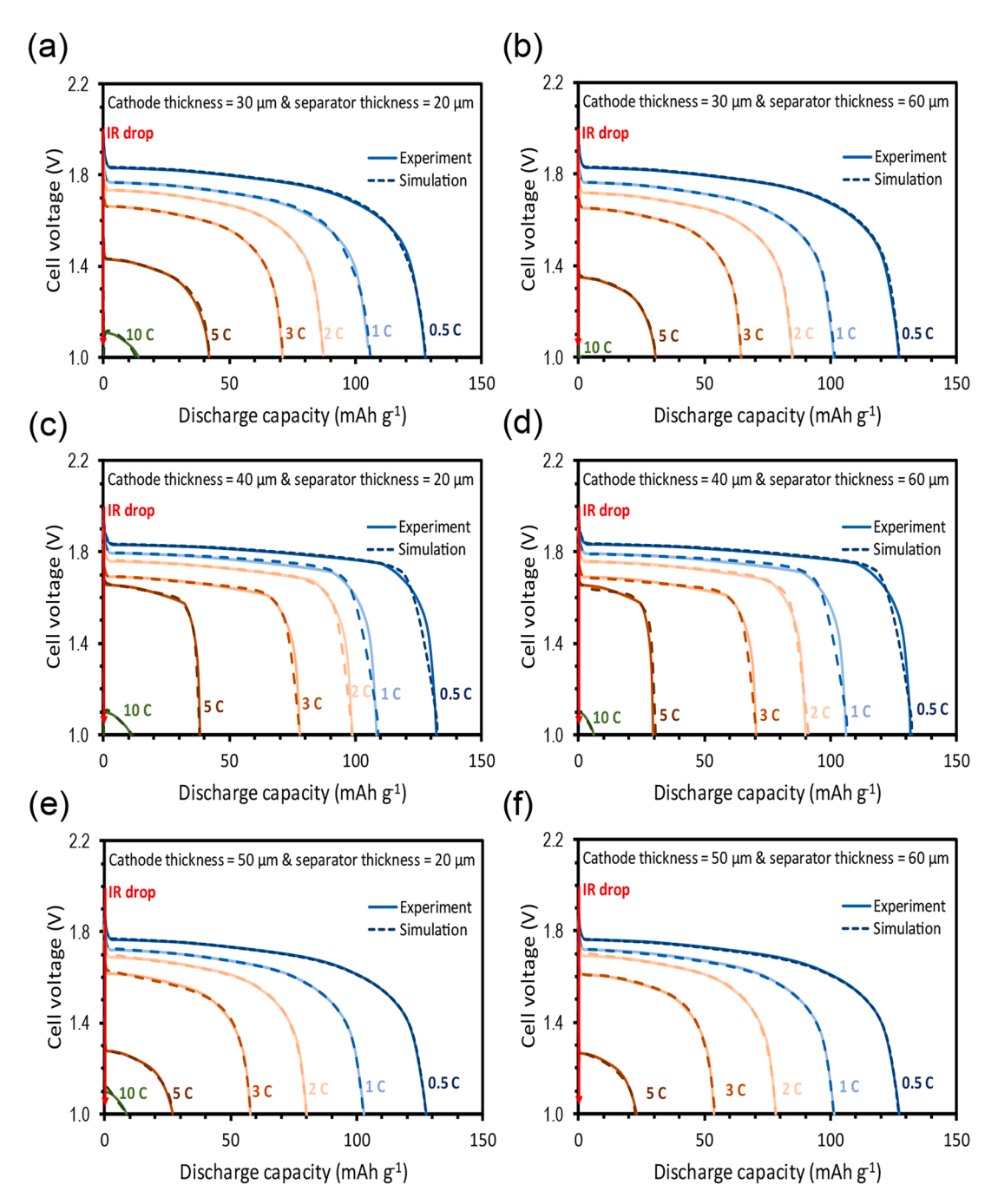


Fig. 3. Model best fit for cells with different cathode and separator thicknesses of 20 μm and 60 μm. Simulated and experimental discharge profiles of cells with cathode thickness of (a), (b) 30 μm, (c), (d) 40 μm and (e), (f) 50 μm.

(Fig. 5a and b, c and d, e and f), increasing the thickness of the separator resulted in a reduction in the depth of intercalated Li ions in the cathode, that is the size of the concentrated region reduced. However, there were no significant changes in the size of the concentrated region for the cells with similar separator thickness and varying cathode thickness (Fig. 5a, c, e and b, d, f). For the cells with a separator thickness of 20 μm , almost all the Li ions in the cells with a cathode thickness of 30 μm , and 40 μm , deintercalated the anode to the cathode (Fig. 5a and b) at the end of this discharge. However, the amount of Li ion that deintercalated the anode decreased as the cathode thickness was increased to 50 μm . A similar observation was made in the cells with a separator thickness of 60 μm (Fig. 5d and f) except for the cells with a cathode thickness of 30 μm . In principle, more Li ion should be extracted from the cells with low cathode thickness, however, due to the poor contacts between the active

materials and conductors in thinner electrodes [38], most of Li ions still remained in the anode at the end of the discharge as observed in Fig. 5b. From Fig. 5, the concentration of Li in the solid phase in the anode was near depletion for the cells with a cathode and separator thickness of 30 μm and 20 μm (Fig. 5a), 40 μm and 20 μm (Fig. 5c), and 40 μm and 60 μm (Fig. 5d). Thus solid-phase diffusion limitations occur at high current rate in Li ion batteries, and it is strongly influenced by the design of the cell.

4.5. Effects of cell design parameters on specific capacity

To demonstrate the predictability of the experimentally validated model, we simulated the effect of various electrode thicknesses and porosities on the specific capacity in 1D as a function of the separator W.A. Appiah et al.

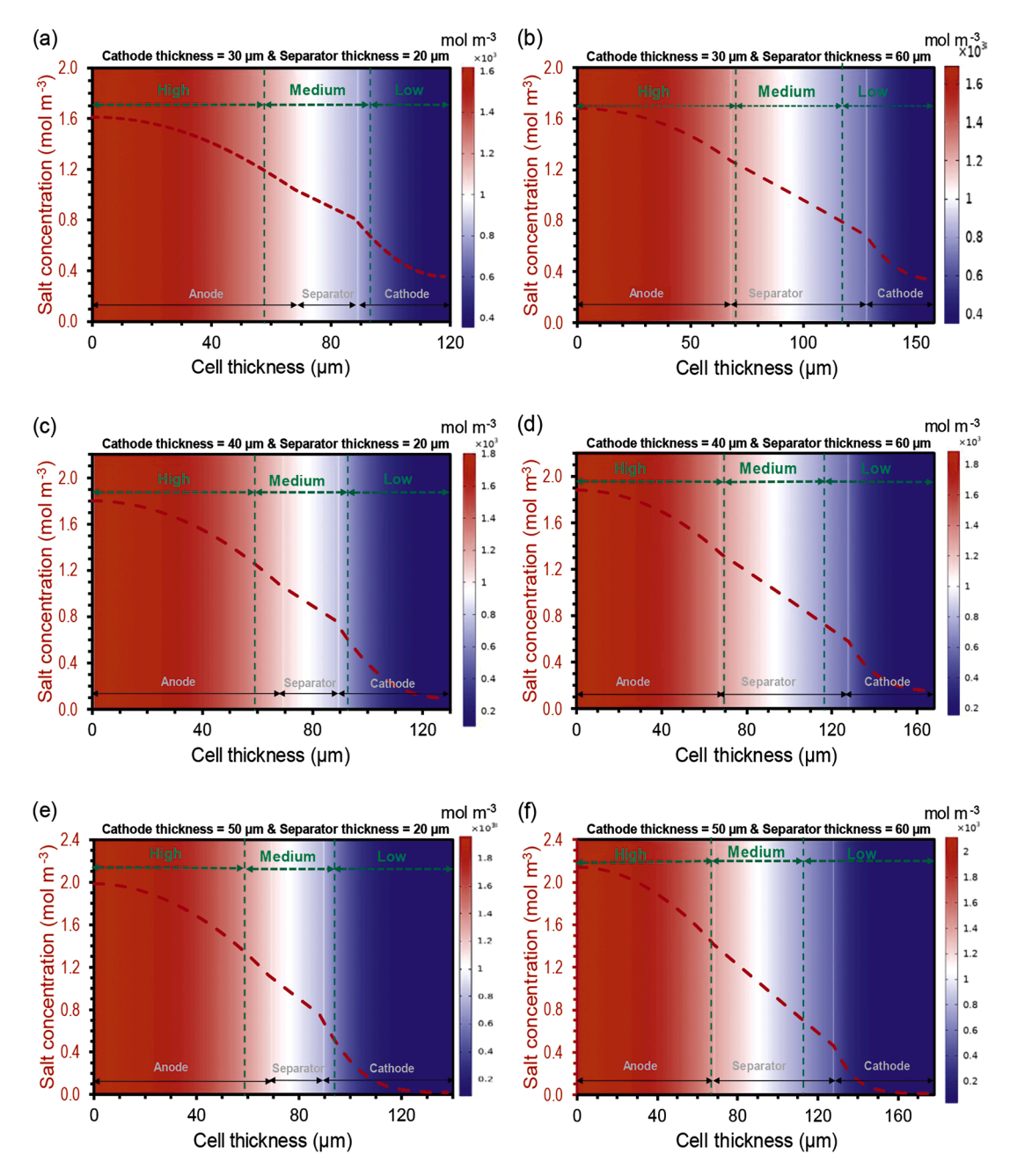


Fig. 4. Effects of cell design parameters on the electrolyte salt concentration. Simulated salt concentration at the end of discharge for a discharge current rate of 10 C for cells with cathode and separator thickness of (a) 30 μ m and 20 μ m, (b) 30 μ m and 60 μ m (c) 40 μ m and 20 μ m (d) 40 μ m and 60 μ m (e) 50 μ m and 20 μ m, and (f) 50 μ m and 60 μ m, respectively.

thickness at discharge current rate of 1C and 5C and presented the outcome in Fig. 6. The thickness of cathode, separator and anode were varied from of 20 μm to 100 μm , 20 μm to 60 μm , and 20 μm to 100 μm , respectively. The porosities of the cathode and anode were varied within the ranges of 0.2 and 0.5. All the other parameters (Table 1) were held constant when varying the parameters in Fig. 6. Increasing the thickness of the separator did not result in any significant changes in the specific capacity of the cell at a low c-rate of 1C but varied slightly at higher c-rate of 5C in all the four cases considered. Increasing the thickness of the cathode, resulted in an increase in the specific capacity until an optimized value of 80 μm and 40 μm at 1C and 4C respectively (Fig. 6a). A similar trend was observed for the changes in the thickness of the anode in Fig. 6b. However, the specific capacity increased linearly with an increase in the thickness of anode at 1C and no specific capacity was

observed in the cells with thin anodes (20 μm and 40 μm) at 5C because the anode is the limiting electrode and at high c-rates the amount of accumulated Li ions are not enough to be readily transported to the cathode in a short time. The drop in the specific capacity with an increase in the electrode thickness is due to diffusion limitations for the Li ions and this effect is more pronounced at high current rates. A near flat surface was observed at 5C when both the cathode and anode porosities were varied at 5C in Fig. 6c and d respectively indicating no significant effect of the electrode porosity on the specific capacity at high c-rate. Nevertheless, the specific capacity increased with a decrease in the electrode porosities in Fig. 6c and d at 1C due to the increase in the volume fraction of the active materials in the electrodes.

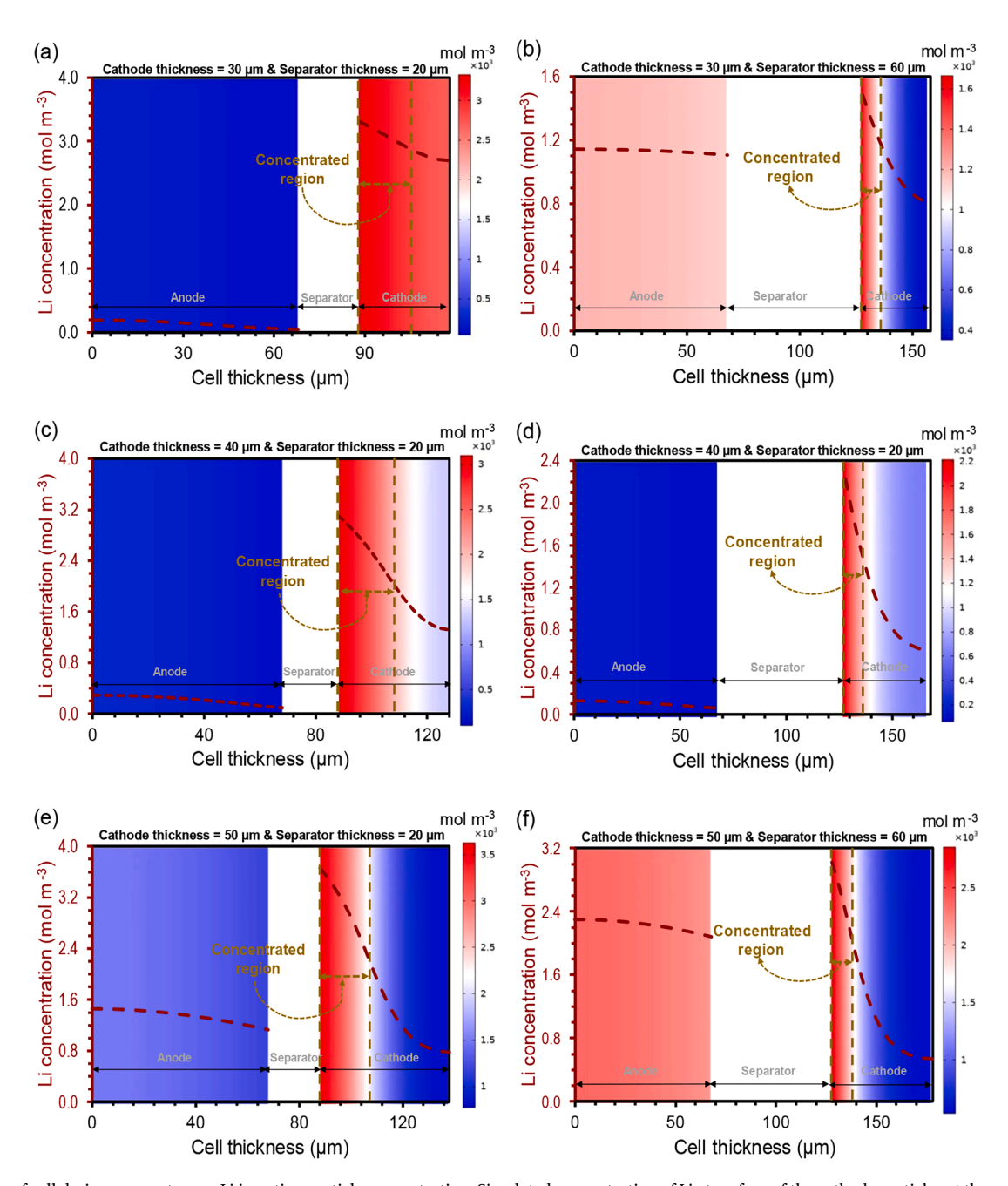


Fig. 5. Effects of cell design parameters on Li insertion particle concentration. Simulated concentration of Li at surface of the cathode particles at the end of discharge for a discharge current rate of 10 C for cells with cathode and separator thickness of (a) 30 μ m and 20 μ m, (b) 30 μ m and 60 μ m (c) 40 μ m and 20 μ m and 20 μ m, and (f) 50 μ m and 60 μ m, respectively.

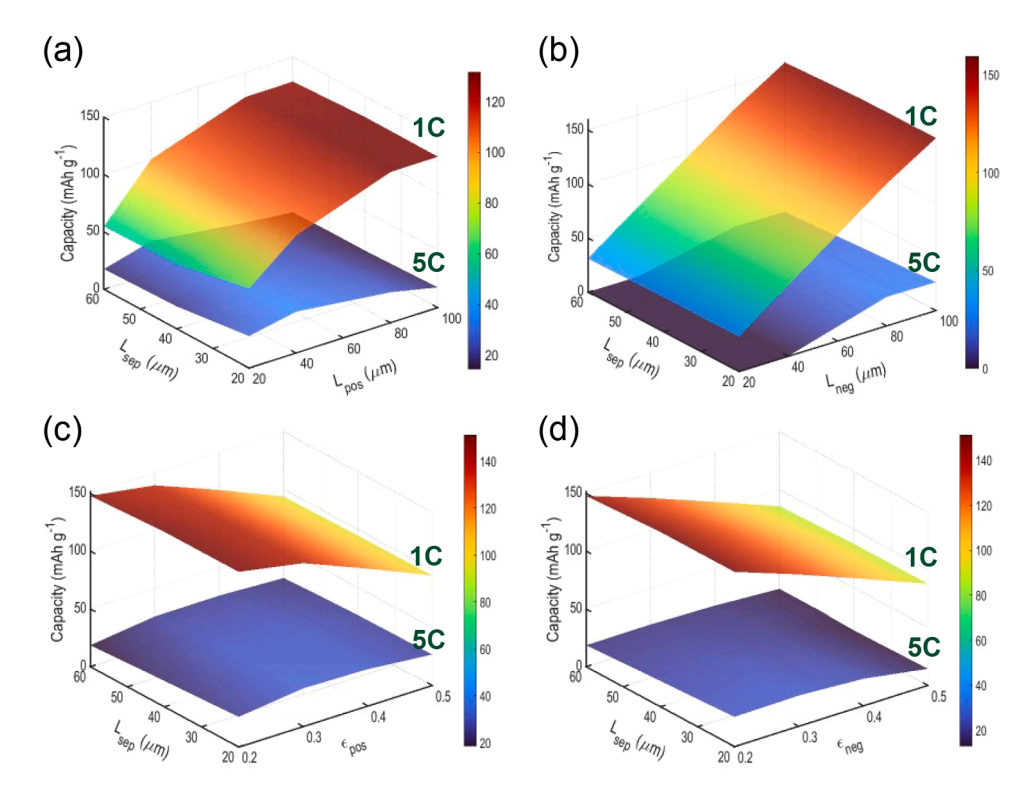


Fig. 6. Effect of cell design parameters on specific capacity. Specific capacity as a function of thickness of the separator and (a) cathode thickness and (b) anode thickness, (c) cathode porosity, and (d) anode porosity, at discharge current rates of 1C and 5C. The simulations were performed in 1D.

5. Conclusion

We simulated the electrochemical performance of a lithium-ion cell composed of LiFePO $_4$ cathode, Li $_4$ Ti $_5$ O $_{12}$ anode and a porous separator filled with a liquid electrolyte using an experimentally validated pseudotwo-dimensional model (P2D). The results are presented in both 2D and 1D to enable a direct visualization of the effect of the effect electrode design parameters on the distribution of Li ions in the electrode. From our simulation, we derived two significant observations.

- Increasing the thickness of the separator inhibits the cell performance at high discharge current rates above 5C but does not show any significant effect at low current rates.
- 2. The major factor inhibiting the performance in the thick electrodes at high current rate is solution phase diffusion limitations and the limiting electrode is the anode.

The results and the model (readily available as an app) presented here can serve as a guide to researchers and industries to develop and optimize electrode design parameters to accelerate the production of batteries.

CRediT authorship contribution statement

Williams Agyei Appiah: Writing – review & editing, Writing – original draft, Methodology, Investigation, Formal analysis, Data curation, Conceptualization. Dohwan Kim: Data curation. Yong Min Lee: Writing – original draft, Supervision, Data curation. Juan Maria Garcia-Lastra: Writing – review & editing, Supervision. Ivano E. Castelli: Writing – review & editing, Writing – original draft, Project administration, Funding acquisition, Conceptualization.

Declaration of competing interest

The authors declare that they have no known competing financial interests or personal relationships that could have appeared to influence the work reported in this paper.

Data availability

Data will be made available on request.

Acknowledgements

The authors acknowledge support from the Department of Energy Conversion and Storage, Technical University of Denmark through the Technology Track Battery project "Design and Printing of Solid-state Batteries (DeSSB)" and, the European Union's Horizon 2020 research and innovation program under grant agreement No 957189 (BIG-MAP) and No 957213 (BATTERY2030PLUS).

References

- R. Schmuch, R. Wagner, G. Hörpel, T. Placke, M. Winter, Performance and cost of materials for lithium-based rechargeable automotive batteries, Nat. Energy 3 (4) (2018) 267–278. https://doi.org/10.1038/s41560-018-0107-2.
- [2] B. Nykvist, M. Nilsson, Rapidly falling costs of battery packs for electric vehicles, Nat. Clim. Chang 5 (4) (2015) 329–332, https://doi.org/10.1038/nclimate2564.
- [3] V. Etacheri, R. Marom, R. Elazari, G. Salitra, D. Aurbach, Challenges in the development of advanced Li-ion batteries: a review, Energy Environ. Sci. 4 (2011) 3243–3262
- [4] J. Liu, Z. Bao, Y. Cui, E.J. Dufek, J.B. Goodenough, P. Khalifah, Q. Li, B.Y. Liaw, P. Liu, A. Manthiram, Y.S. Meng, V.R. Subramanian, M.F. Toney, V. V. Viswanathan, M.S. Whittingham, J. Xiao, W. Xu, J. Yang, X.Q. Yang, J.G. Zhang, Pathways for practical high-energy long-cycling lithium metal batteries, Nature Energy 4 (3) (2019) 180–186, https://doi.org/10.1038/s41560-019-0338-x.
- [5] W.A. Appiah, J. Park, S. Song, S. Byun, M.H. Ryou, Y.M. Lee, Design optimization of LiNi0.6Co0.2Mn0.2O2/graphite lithium-ion cells based on simulation and

- experimental data, J. Power Sources 319 (2016) 147–158, https://doi.org/10.1016/j.jpowsour.2016.04.052.
- [6] C. Heubner, A. Nickol, J. Seeba, S. Reuber, N. Junker, M. Wolter, M. Schneider, A. Michaelis, Understanding thickness and porosity effects on the electrochemical performance of LiNi0.6Co0.2Mn0.2O2-based cathodes for high energy Li-ion batteries, J. Power Sources 419 (2019) 119–126, https://doi.org/10.1016/J. JPOWSOUR.2019.02.060.
- [7] V. Srinivasan, J. Newman, Design and optimization of a natural graphite/iron phosphate lithium-ion cell, J. Electrochem. Soc. 151 (2004) A1530–A1538.
- [8] M. Singh, J. Kaiser, H. Hahn, Thick electrodes for high energy lithium ion batteries,
 J. Electrochem. Soc. 162 (2015) A1196–A1201, https://doi.org/10.1149/ 2.0401507JES/XMI.
- [9] B.-S. Lee, Z. Wu, V. Petrova, X. Xing, H.-D. Lim, H. Liu, P. Liu, Analysis of ratelimiting factors in thick electrodes for electric vehicle applications, J. Electrochem. Soc. 165 (2018) A525–A533, https://doi.org/10.1149/2.0571803JES/XML.
- [10] Z. Li, L. Yin, G.S. Mattei, M.R. Cosby, B.S. Lee, Z. Wu, S.M. Bak, K.W. Chapman, X. Q. Yang, P. Liu, P.G. Khalifah, Synchrotron operando depth profiling studies of state-of-charge gradients in thick Li(Ni0.8Mn0.1Co0.1)O2 cathode films, Chem. Mater. 32 (2020) 6358–6364, https://doi.org/10.1021/ACS. CHEMMATER.0C00983/SUPPL_FILE/CM0C00983_SI_003.TXT.
- [11] M. Zhang, M. Chouchane, S.A. Shojaee, B. Winiarski, Z. Liu, L. Li, R. Pelapur, A. Shodiev, W. Yao, J.M. Doux, S. Wang, Y. Li, C. Liu, H. Lemmens, A.A. Franco, Y. S. Meng, Coupling of multiscale imaging analysis and computational modeling for understanding thick cathode degradation mechanisms, Joule 7 (2023) 201–220, https://doi.org/10.1016/J.JOULE.2022.12.001.
- [12] Z. Chen, D.L. Danilov, R.A. Eichel, P.H.L. Notten, Porous electrode modeling and its applications to Li-ion batteries, Adv. Energy Mater. 12 (2022) 2201506, https://doi.org/10.1002/AENM.202201506.
- [13] D. Diddens, W.A. Appiah, Y. Mabrouk, A. Heuer, T. Vegge, A. Bhowmik, D. Diddens, Y. Mabrouk, A. Heuer, W.A. Appiah, T. Vegge, A. Bhowmik, Modeling the solid electrolyte interphase: machine learning as a game changer? Adv. Mater. Interfaces 9 (2022) 2101734 https://doi.org/10.1002/ADMI.202101734.
- [14] D. Atkins, E. Ayerbe, A. Benayad, F.G. Capone, E. Capria, I.E. Castelli, I. Cekic-Laskovic, R. Ciria, L. Dudy, K. Edström, M.R. Johnson, H. Li, J.M.G. Lastra, M.L. De Souza, V. Meunier, M. Morcrette, H. Reichert, P. Simon, J.P. Rueff, J. Sottmann, W. Wenzel, A. Grimaud, Understanding battery interfaces by combined characterization and simulation approaches: challenges and perspectives, Adv. Energy Mater. 12 (2022) 2102687. https://doi.org/10.1002/AENM.202102687.
- [15] V. Ramadesigan, P.W.C. Northrop, S. De, S. Santhanagopalan, R.D. Braatz, V. R. Subramanian, Modeling and simulation of lithium-ion batteries from a systems engineering perspective, J. Electrochem. Soc. 159 (2012) R31, https://doi.org/10.1149/2.018203.FS.
- [16] A. Jokar, B. Rajabloo, M. Désilets, M. Lacroix, Review of simplified Pseudo-two-Dimensional models of lithium-ion batteries, J. Power Sources 327 (2016) 44–55, https://doi.org/10.1016/j.jpowsour.2016.07.036.
- [17] M.A. Hannan, M.S.H. Lipu, A. Hussain, A. Mohamed, A review of lithium-ion battery state of charge estimation and management system in electric vehicle applications: challenges and recommendations, Renew. Sustain. Energy Rev. 78 (2017) 834–854, https://doi.org/10.1016/J.RSER.2017.05.001.
- [18] E. Sarasketa-Zabala, E. Martinez-Laserna, M. Berecibar, I. Gandiaga, L. M. Rodriguez-Martinez, I. Villarreal, Realistic lifetime prediction approach for Liion batteries, Appl. Energy 162 (2016) 839–852, https://doi.org/10.1016/J. APNERGY 2015 10 115
- [19] H. Zhou, L.T. Gao, Y. Li, Y. Lyu, Z.S. Guo, Electrochemical performance of lithiumion batteries with two-layer gradient electrode architectures, Electrochim. Acta 476 (2024) 143656, https://doi.org/10.1016/J.ELECTACTA.2023.143656.
- [20] M. Magri, B. Boz, L. Cabras, A. Salvadori, Quantitative investigation of the influence of electrode morphology in the electro-chemo-mechanical response of liion batteries, Electrochim. Acta 405 (2022) 139778, https://doi.org/10.1016/J. ELECTACTA.2021.139778.

- [21] W.A. Appiah, A. Stark, S. Lysgaard, J. Busk, P. Jankowski, J.H. Chang, A. Bhowmik, B. Gollas, J.M. Garcia-Lastra, Unveiling the plating-stripping mechanism in aluminum batteries with imidazolium-based electrolytes: a hierarchical model based on experiments and ab initio simulations, Chem. Eng. J. 472 (2023) 144995, https://doi.org/10.1016/J.CEJ.2023.144995.
- [22] C. von Lüders, J. Keil, M. Webersberger, A. Jossen, Modeling of lithium plating and lithium stripping in lithium-ion batteries, J. Power Sources 414 (2019) 41–47, https://doi.org/10.1016/J.JPOWSOUR.2018.12.084.
- [23] X. Zhao, Y. Yin, Y. Hu, S.-Y. Choe, Electrochemical-thermal modeling of lithium plating/stripping of Li(Ni0.6Mn0.2Co0.2)O2/Carbon lithium-ion batteries at subzero ambient temperatures, J. Power Sources 418 (2019) 61–73, https://doi. org/10.1016/J.JPOWSOUR.2019.02.001.
- [24] J. Li, B. Liu, S. Li, D. Hu, L. Wang, J. Xu, Mechanistic modeling of Li plating in lithium-ion batteries, J. Power Sources 521 (2022) 230936, https://doi.org/ 10.1016/J.JPOWSOUR.2021.230936.
- [25] V. Srinivasan, J. Newman, Discharge model for the lithium iron-phosphate electrode, J. Electrochem. Soc. 151 (2004) A1517, https://doi.org/10.1149/ 1.1785012/XMI.
- [26] M. Xu, B. Reichman, X. Wang, Modeling the effect of electrode thickness on the performance of lithium-ion batteries with experimental validation, Energy 186 (2019) 115864, https://doi.org/10.1016/J.ENERGY.2019.115864.
- [27] Y. Li, Z. Tan, Effects of a separator on the electrochemical and thermal performances of lithium-ion batteries: a numerical study, Energy Fuels 34 (2020) 14915–14923, https://doi.org/10.1021/ACS.ENERGYFUELS.0C02609.
- [28] W.A. Appiah, D. Kim, Y.M. Lee, J.M. Garcia-Lastra, I.E. Castelli, A physics-based model application for designing LiFePO4/Li4Ti5O12 (LFP/LTO) battery cells, DTU Data (2023), https://doi.org/10.11583/DTU.23975607.
- [29] M. Doyle, T.F. Fuller, J. Newman, Modeling of galvanostatic charge and discharge of the lithium/polymer/insertion cell, J. Electrochem. Soc. 140 (1993) 1526, https://doi.org/10.1149/1.2221597.
- [30] J. Newman, W. Tiedemann, Porous-electrode theory with battery applications, AIChE J. 21 (1975) 25–41.
- [31] W. Agyei Appiah, J. Park, S. Byun, Y. Roh, M. Ryou, Y.M. Lee, Time-effective accelerated cyclic aging analysis of lithium-ion batteries, ChemElectroChem 6 (2019) 3714–3725, https://doi.org/10.1002/celc.201900748.
- [32] W.A. Appiah, D. Kim, J. Song, M. Ryou, Y.M. Lee, Understanding the effect of polydopamine interlayer on the long-term cycling performance of silicon anodes: a multiphysics-based model study, Batteries Supercaps 2 (2019) batt.201900019, https://doi.org/10.1002/batt.201900019.
- [33] U.S. Kasavajjula, C. Wang, P.E. Arce, Discharge model for LiFePO[sub 4] accounting for the solid solution range, J. Electrochem. Soc. 155 (2008) A866, https://doi.org/10.1149/1.2980420.
- [34] S.T. Taleghani, B. Marcos, K. Zaghib, G. Lantagne, A study on the effect of porosity and particles size distribution on li-ion battery performance, J. Electrochem. Soc. 164 (2017) 3179–3189, https://doi.org/10.1149/2.0211711jes.
- [35] S. Santhanagopalan, Q. Guo, P. Ramadass, R.E. White, Review of models for predicting the cycling performance of lithium ion batteries, J. Power Sources 156 (2006) 620–628, https://doi.org/10.1016/J.JPOWSOUR.2005.05.070.
- [36] W.A. Appiah, Y. Roh, C.B. Dzakpasu, M.-H. Ryou, Y.M. Lee, Design of thin-film interlayer between silicon electrode and current collector using a chemomechanical degradation model, J. Electrochem. Soc. 167 (2020) 080542, https:// doi.org/10.1149/1945-7111/ab9382.
- [37] J. Park, W.A. Appiah, S. Byun, D. Jin, M.H. Ryou, Y.M. Lee, Semi-empirical long-term cycle life model coupled with an electrolyte depletion function for large-format graphite/LiFePO4 lithium-ion batteries, J. Power Sources 365 (2017) 257–265, https://doi.org/10.1016/J.JPOWSOUR.2017.08.094.
- [38] J. Jeong, H. Lee, J. Choi, M.H. Ryou, Y.Min Lee, Effect of LiFePO4 cathode density and thickness on electrochemical performance of lithium metal polymer batteries prepared by in situ thermal polymerization, Electrochim. Acta 154 (2015) 149–156, https://doi.org/10.1016/J.ELECTACTA.2014.12.051.